www.sciencemag.org/cgi/content/full/science.1216937/DC1

Supporting Online Material for

Influence of Synaptic Vesicle Position on Release Probability and Exocytotic Fusion Mode

Hyokeun Park, Yulong Li, Richard W. Tsien*

*To whom correspondence should be addressed. E-mail: rwtsien@stanford.edu

Published 16 February 2012 on *Science* Express
DOI: 10.1126/science.1216937

This PDF file includes

Materials and Methods

Three-dimensional microscopy setup

A three-dimensional microscopy setup was built as previously described (*9*) with minor modifications. An inverted epi-fluorescence microscope (Ti-S, Nikon, Japan), equipped with custom-built dual-focus imaging optics, and an electron multiplying (EM) CCD camera (Ixon+, Andor, N. Ireland) were used to capture fluorescence signals (Fig. S1A). An oil immersion 100x apochromat objective (Nikon, Japan) was used, and the pixel size in image was 160 nm in the x-y plane. Custom-written IDL coded programs were used to fit a two-dimensional Gaussian function to the original fluorescence signal to locate two-dimensional centroid and to calculate the fluorescence peak intensity at two different focal planes (I_1, I_2). A piezo actuator (PIFOC, Physik Instrumente (PI), Karlsruhe/Palmbach, Germany) was used to generate a calibration curve based on the z-position dependence of the relative peak intensity difference $((I_1-I_2)/(I_1+I_2))$. Several programs written in LabVIEW (National Instruments, Austin, TX) were used to control a piezo actuator and acquire data on the z-position. Z-positions of objects were calculated from relative peak intensity difference by means of the empirically determined calibration curve, as in (*9*). A 405 nm laser (Crystalaser, Reno, NV) was used to illuminate streptavidin-coated quantum dots (Qdots). A 10X beam expander (Beamexpander, Canton, MA) and focus lens were used to illuminate the sample uniformly.

Cell culture and transfection

Rat hippocampal neurons were cultured as previously described (*5*, *23*) in accordance with our animal protocol approved by the Stanford University Administrative Panel on Laboratory Animal Care. Transfection of PSD-95-GFP was performed by the calcium phosphate method at DIV 10 as described in (*24*).

Real-time imaging of single Qdots in cultured hippocampal neurons

Experiments were performed at room temperature between DIV 14 and DIV 21. A dichroic mirror (z405rdc, Chroma, Bellows Falls, VT) and an emission filter (ET605/70m, Chroma) were used to capture the specific fluorescence of Qdots. Two different emission filters (ET525/50m and HQ665LP, Chroma) were used to capture the fluorescence signal from PSD-95-GFP and FM 4-64 respectively. Chromatic aberrations were corrected as described in (*25*). Streptavidin-coated Qdots (A10196, Life Technologies, Eugene, OR), with a diameter of ~18 nm (based on information provided by Life Technologies), were preincubated at room temperature for ~1 h with biotinylated antibodies (Cat No.105 311BT, Synaptic System, Göttingen, Germany) binding to the luminal domain of synaptotagmin 1 at a 1:1 ratio, before addition of the conjugates solution to the sample chamber. The final concentration of antibody-conjugated Qdots was limited to 0.1 nM to label sparsely (on average, less than one Qdot per bouton). Similar experimental conditions and methods were used to prepare Qdots conjugated with biotinylated VGAT antibodies (a gift from Dr. Henrik Martens of Synaptic System). These were also used at a final concentration of 0.1 nM, just as with biotinylated synaptotagmin 1 antibody-conjugated Qdots. In addition to Tyrode solution, the preincubation solution contained 2.5 mM DDT (D9779, Sigma-Aldrich, St. Louis, MO) and 0.04 mg/ml casein (C3400, Sigma-Aldrich) to increase the photostability of the Qdots and to prevent nonspecific binding. After addition of preincubation solution to the sample chamber, neurons were stimulated with platinum electrodes connected to the Grass Stimulator (SD9, Grass Technologies, West Warwick, RI), at 10 Hz for 1 s or 120 s. Then, neurons were incubated for 60 s without stimulation, followed by extensive washing for 20 min using a superfusion system. Then, 1 μM trypan blue (TB) (T8154, Sigma-Aldrich) was applied within ~1 min before initiation of imaging, to avoid depletion of vesicular glutamate following possible block of glutamate uptake into vesicles(*26*). The solution switching time was ~5 s. FM 4-64 and PSD-95-GFP were imaged first, before continuous imaging of Qdots at 10 Hz (exposure time of

~100 ms) for 160 s. This imaging period consisted of 20 s without stimulation, then 120 s of 10 Hz stimulation, and a final 20 s without stimulation. Synchronization of the stimulator, beam shutter and EMCCD camera was performed with a triggering signal from the camera, driving a Digidata 1322A (Molecular Devices, Sunnyvale, CA), which in turn synchronized stimulation. A Clampex program (Molecular Devices) was used to generate the stimulation protocol. For the FM 4-64 destaining experiments, the final concentration of ~10 μM FM 4-64 (T3166, Life Technologies) was used. The loading protocol was the same as that used for Qdot loading, except that 1200 APs (10 Hz for 120 s) were used to stain the whole recycling pool and images were taken for 160 s at 1 Hz (exposure time of ~100 ms). Cells were superfused with Tyrode solution (containing 150 mM NaCl, 4 mM KCl, 2 mM $CaCl_2$, 2 mM $MgCl_2$, 10 mM glucose, 10 mM HEPES, 310–315 mOsm, with pH set at 7.30 with NaOH). All solutions contained 5 μM NBQX (Ascent Scientific, Princeton, NJ) and 50 μM D-APV (Ascent Scientific) to prevent recurrent activity and synaptic plasticity. Fluorescence quenching measurements of Qdots in a cuvette were performed using a fluorescence spectrophotometer (F-4500, Hitachi High-Tech, Tokyo, Japan) kindly provided by Prof. Axel Brunger.

Analysis

Student's *t*-test was performed using a custom-written IDL coded program (*27*, *28*) to detect the movement of vesicles and the decrease in the fluorescence of Qdots associated with exocytosis. Metamorph (Molecular Devices) was used to calculate the fluorescence of the Qdot within the region-of-interest (ROI). χ^2 tests were performed by moving a variable separator in 0.1 s increments and the other separator in 0.001 increments of the unquenched fraction using a custom-written MATLAB program. NCSS (NCSS, Kaysville, UT) and Graphpad Prism (GraphPad Software, La Jolla, CA) were used for statistical analysis. Origin (OriginLab, Northampton, MA) and Sigmaplot (Systat Software, San Jose, CA) were used for fitting.

In vitro fluorescence assay of single Qdots

Sample chambers were prepared as described in (*29*). After assembling the sample chamber, we introduced 100 μL of 1 mg/mL biotinylated bovine serum albumin (BSA) (A8549, Sigma) in Tyrode and allowed the solution to remain for 5 min before a wash with 100 μL of Tyrode solution. Next, 100 μL of 0.1 nM streptavidin-coated Qdot (A10196, Life Technologies) in Tyrode was added and allowed to reside for 5 min before further washing with 100 μL of Tyrode. For the quenching experiment, 100 μL of 1 μM TB was added. In order to determine whether there was an observable spectral shift with our system, fluorescence was collected with a longpass emission filter (HQ500LP, Chroma), to compare with results obtained with a standard emission filter for Qdots (ET605/70m, Chroma). The experiments were performed with the same setup as that used for three-dimensional tracking of vesicles in living neurons. The imaging was performed at 10 Hz (exposure time of ~100 ms) for 160 s, identical to the protocol used for living neuron imaging. Metamorph (Molecular Device) was used to calculate the fluorescence of a single Qdot in the same way as used for single Qdots in living neurons. The identification of a single Qdot was based on observations of photoblinking events, seen as a sudden and reversible drop in fluorescence to zero intensity.

SOM Text

Detailed explanation of three-dimensional (3D) microscopy

The scheme of our 3D microscopy setup with dual-focus imaging optics (modified from a published design (*9*)) is shown in Fig. S1A. Dual-focus imaging optics consist of an aperture(A), a beam splitter (BS), lenses (L), mirrors (M) and a right angle mirror (RAM); a beam splitter divides the fluorescence signal from the biological specimen into two beams, each with its own plane of focus, determined by independent lenses. The two fluorescence images are captured side-by-side by an EM CCD camera. Object displacement along the z-axis is visualized as opposing changes in fluorescence intensity in the two planes (Fig. S1B). The typical separation between the two focal planes was ~1 μm in our setup. A quantitative index for z-axis position is provided by the normalized difference between peak intensity $(I_1-I_2)/(I_1+I_2)$, where I_1 and I_2 are the fitted peak intensity in plane 1 and 2. To find the z-axis position, we generated a calibration curve by moving a sample chamber along the z-axis (Fig. S1C). This standard curve for $(I_1-I_2)/(I_1+I_2)$ allowed us to determine the z-position of objects. The standard deviation (σ) of the z-localization distribution was 12.3 nm for 10 Hz imaging (Fig. 1A) and the accuracy of our system (2.35σ) was ~30 nm, corresponding to the full-width at half maximum (FWHM). The accuracy of x- and y-localization was ~20 nm (Fig. 1A).

Quantitative analysis of fluorescence decrease by quenching

Quantitative analysis of the decrease in fluorescence relied on automated detection of downward steps, performed by a custom-written IDL program that utilizes a *t*-test algorithm (*27, 28*) with $p<0.05$ as a criterion. Results from 41 experiments revealed two distinct patterns of behavior. In one set of results, representing K&R (red circles in Fig. S5B), the partial quenching sojourns lasted at least 4 s (shortest, 4 s; median, 8.8 s; average, 15.0±2.5 s (SEM), n = 30), with the unquenched fractions averaging 0.281±0.016 (SEM). This average corresponds to a mean TB concentration of 0.2 μM inside single vesicles, determined according to the *in vitro* quenching curve (Fig. 1E). In the remaining experiments (attributed to FCF, data in blue triangles in Fig. S5B), the algorithm was either unable to detect an intermediate step (n = 19), or reported an apparent sojourn with a duration of <2 s (average, 0.9±0.1 s, n = 22) (see the example of this apparent sojourn in Fig. S5A). When detectable, this brief sojourn likely represents the last phase of FCF, when the Qdot was fully exposed to TB, but just before its movement away from the ROI. In order to investigate whether this apparent sojourn was clearly separated from the partial quenching sojourn, we performed χ^2 tests with variable separators of dwell times and unquenched fractions. χ^2 has a maximum value (37.3, $p<10^{-8}$) at a separator dwell time between 1.9 s and 4 s (Fig. S5B, S5C), supporting the use of this interval to distinguish between the partial quenching of K&R and the apparent sojourns associated with FCF. The unquenched fraction of these sojourns averaged 0.124±0.011 (SEM) (n=22), very close to the value expected from cuvette measurements (0.137±0.003 (SEM), n=3).

Partial quenching as an indicator of K&R

A key to verifying that the partial entry of the quencher did indeed indicate K&R fusion was a reduction in the extracellular quencher concentration. If the fusion pore is only open for a limited duration in K&R, lowering the extracellular level of the quencher should decrease quencher entry and the overall degree of quenching (higher F_{TB}/F_0). We confirmed this when we reexamined changes in F_{TB}/F_0 with a 2.5-fold reduction in TB (0.4 μM), by observing a significant reduction in quenching (higher F_{TB}/F_0) for all types of sojourn considered together ($p<0.01$, K-S test) (Fig. S6A): the average unquenched fraction of the partial quenching was 0.351±0.029 (SEM) (n = 14) (Fig. S8), and that of the apparent sojourn was 0.186±0.031 (n = 7), which, once again, is close to the unquenched fraction expected from cuvette measurements (0.211). The average partial quenching fraction at 0.4 μM corresponded to that at 0.1 μM TB inside single vesicles, from

cuvette measurements. Due to the reduction in the rate of quencher entry, the unquenched fraction at 0.4 μM was larger than at 1 μM, and the distribution was more widespread than at 1 μM. Importantly, the prevalence of K&R, and the dwell times (constituting dwell times between successive fusion events and apparent sojourns), were no different with 0.4 μM TB than with 1 μM TB ($p>0.8$, χ^2–test for prevalence, $p>0.2$, K-S test for dwell time)(Fig. S6B). This was as expected if the kinetics of exocytosis and reuse were independent of quencher entry. The strong dependence of the unquenched fraction on the concentration of extracellular TB (Fig. S6A) confirmed that partial quenching reflects a brief opening of the fusion pore and that the level of quencher attained inside the vesicle during a K&R event falls short of a complete equilibration with the external concentration. This approach does not take account of rare instances of prolonged K&R openings. If, for example, the pore stayed open for longer than 10 s (long enough for TB to reach full equilibrium with the outer membrane), but vesicle curvature and identity were preserved, there would be almost complete quenching. We would therefore incorrectly consider the event to be full-collapse fusion, and thus, underestimate the prevalence of K&R, erring on the conservative side. Note, however, the likelihood of such a long opening time would be quite rare in light of previous estimates for the opening time of fusion pores, as <2 s (as determined by capacitance measurements at the calyx synapse, (*30*)), or as ~600 ms, estimated from Qdot experiments (*5*).

In vitro assay of single Qdots fluorescence

In order to investigate whether the decrease in fluorescence that we observed in our system (single Qdot inside a vesicle in living neurons, excited by at our low laser power (<0.5 mW)) was caused by the reported photobleaching or a spectral shift of single Qdots (*31, 32*), we performed an *in vitro* assay of single Qdots fluorescence. We immobilized the streptavidin-conjugated Qdots using biotinylated BSA. The fluorescence of Qdots was measured in our microscopy setup following our standard imaging protocol (10 Hz imaging with an exposure time of ~100 ms). Fig. S9A-1 shows a typical trace of the fluorescence of a single Qdot. The fluorescence showed multiple instances of photoblinking, sometimes approaching zero fluorescence, indicating that the optical signal originated from a single Qdot. The envelope of fluorescence did not decrease, either gradually or abruptly, during our observation time, confirming that a single Qdot did not photobleach in our experimental conditions. The presence of quencher, trypan blue (TB), caused the fluorescence to decrease to 15% (Fig. S9A-2), in agreement with our findings attained with cuvette measurements (Fig. 1E). In order to examine whether there is an observable spectral shift of Qdots in our system, we used a longpass emission filter (HQ500LP), which transmits almost the entire fluorescence of Qdot 625. The typical fluorescence with a longpass filter is shown in Fig. S9B. The fluorescence increased on account of the wider range of transmission, but the steady temporal profile of fluorescence (Fig. S9B) was no different than that obtained with a more conventional emission filter for Qdot (Fig. S9A). This similarity would not have been observed if there had been any observable spectral shift, causing a mismatch between the Qdot emission and the bandpass of the conventional emission filter (ET605/70m). This result indicates that there was no observable spectral shift in our system. Our *in vitro* assays of single Qdot fluorescence confirmed that under our experimental conditions (low laser power (<0.5 mW), observation time, 160 s), there was no sign of photobleaching and spectral shifts, previously reported under less favorable conditions (*32*).

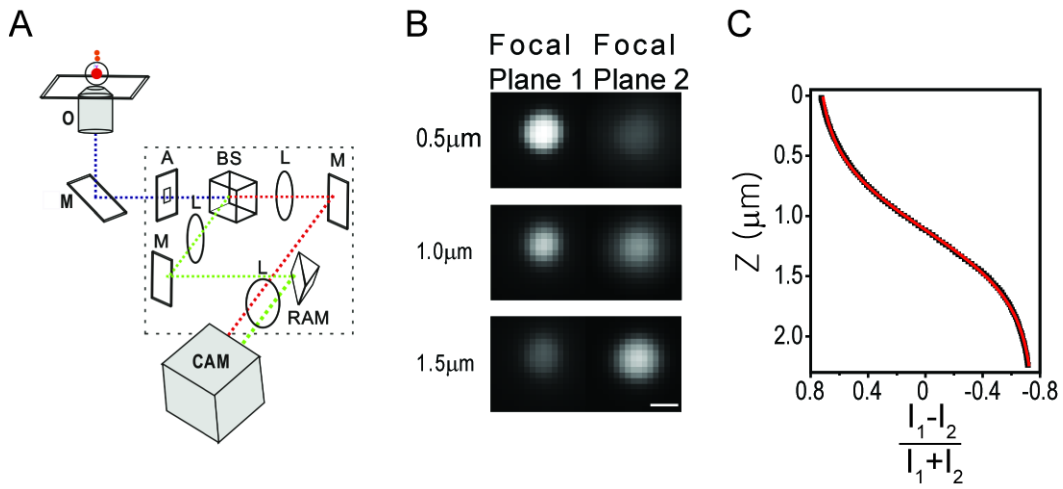

Fig. S1. 3D localization microscopy setup. (A) Dual-focus imaging optics (marked as a dashed square), used to produce two fluorescence images at different focal planes. Basic elements included an aperture (A), a beamsplitter (BS), a right angle mirror (RAM), lenses (L) and mirrors (M). O and M outside a dashed square represent an objective and a mirror in a microscope. (B) Fluorescence images of a Qdots cluster at multiple positions along the z-axis, taken with an EM CCD camera. These images were used to determine peak intensity for the two focal planes. White scale bar, 0.8 µm. (C) A calibration curve was used to locate the position along the z-axis, utilizing the fact that the normalized difference between relative peak intensity, $(I_1-I_2)/(I_1+I_2)$, depends on the z-position. Black squares, experimental data. Red line, fit.

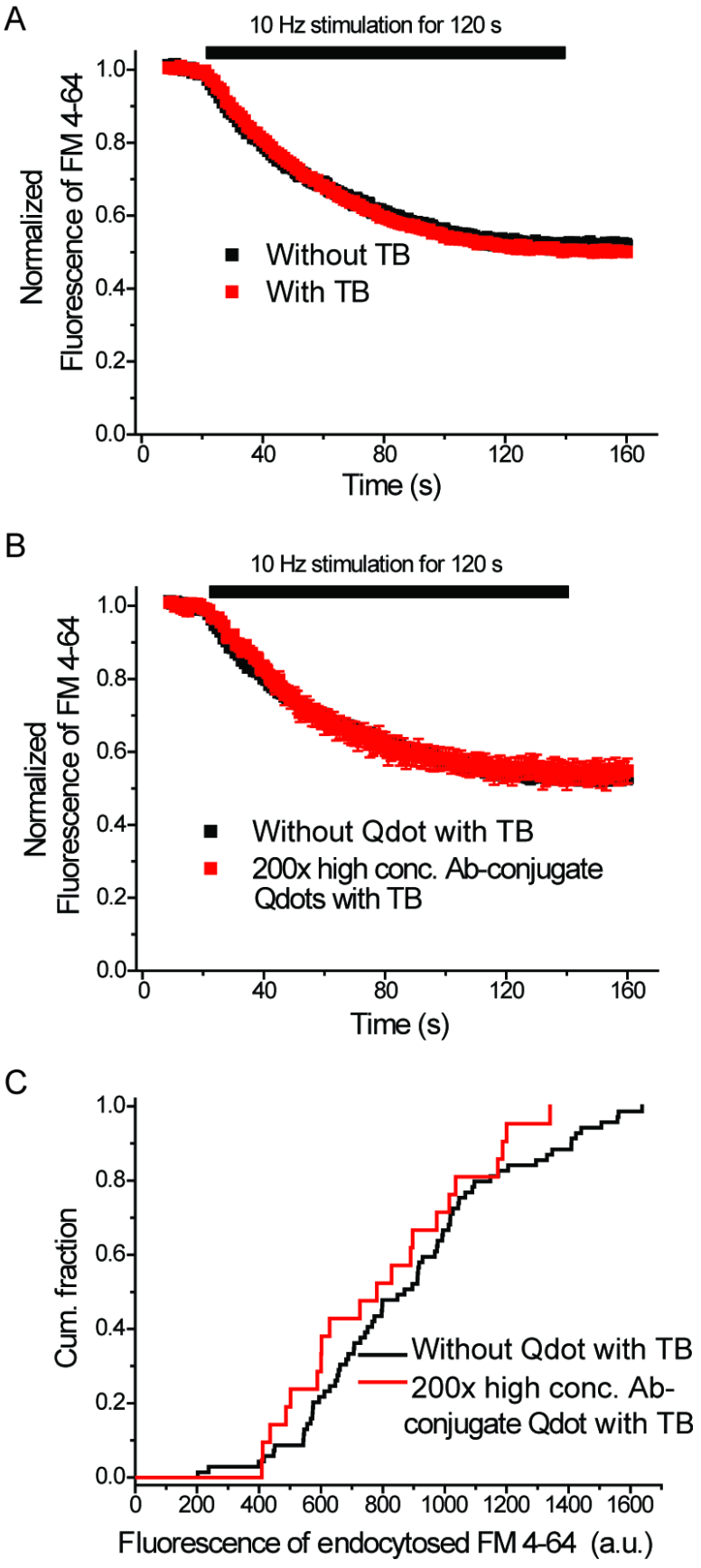
A
10 Hz stimulation for 120 s
Normalized Fluorescence of FM 4-64
1.0
0.8
0.6
0.4
0.2
0.0
0
40
80
120
160
Time (s)
Without TB
With TB
B
10 Hz stimulation for 120 s
Normalized Fluorescence of FM 4-64
Time (s)
Without Qdot with TB
200x high conc. Ab-conjugate Qdots with TB
C
Cum. fraction
0
200
400
600
800
1000
1200
1400
1600
Fluorescence of endocytosed FM 4-64 (a.u.)
Without Qdot with TB
200x high conc. Ab-conjugate Qdot with TB

Fig. S2. Destaining and uptake of FM 4-64 in boutons. (A) FM 4-64 destaining in the absence (black squares) or presence (red squares) of 1 μM TB. 1200 APs were used to destain vesicles in boutons. Following destaining, the normalized fluorescence of FM 4-64 with TB (n=113 boutons) was similar to that without TB (n=58) ($p>0.5$, Student's *t*-test), confirming that TB did not affect the exocytosis of vesicles. This destaining pattern indicates the nearly complete escape of FM 4-64 from vesicles during the opening of the pore, a result similar to that found with FM 2-10 destaining (*33*). This similarity was to be expected insofar as FM 2-10 and FM 4-64 both contain the same side chains. (B) Destaining of FM 4-64 without Qdot (black squares, n=69), or in boutons that had previously been maximally loaded with antibody-conjugated Qdots (red squares, n=21). Prior loading was performed with 1200 APs and with antibody-conjugated Qdots at 20 nM, a concentration 200-fold greater than used in typical experiments, in order to promote probe uptake throughout the total recycling pool. In the 20 nM antibody-conjugate Qdot solution, the content of Qdots, assessed directly with fluorescence measurements, averaged 25±2.4 (SEM) (n=29) per bouton, in line with previous data (*34, 35*). The stimulus-dependent decrease in FM 4-64 fluorescence was not different in the two cases ($p>0.7$, Student's *t*-test), confirming that antibody-conjugated Qdots did not affect the dynamics of exocytosis. (C) The uptake of FM 4-64, determined as the FM 4-64 fluorescence following stimulation, was not different in the absence or presence of 20 nM antibody-conjugate Qdots ($p>0.2$, Student's *t*-test), indicating that the endocytosis was not affected by antibody-conjugated Qdots.

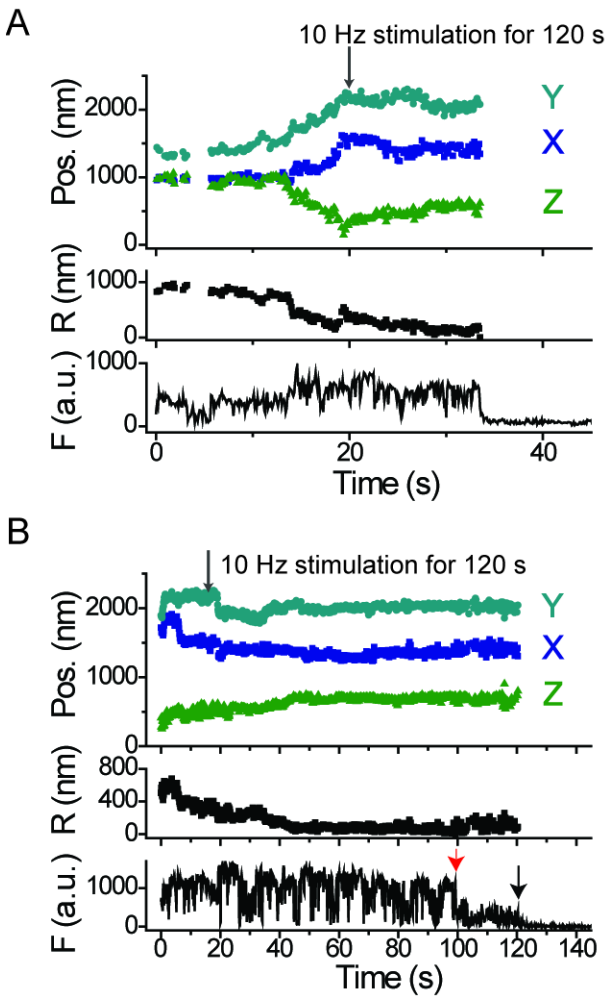

Fig. S3. 3D position and fluorescence of a single VGAT antibody-conjugated Qdot, labeling a single GABAergic vesicle. Photoblinking indicates that the fluorescence trace is that of an individual Qdot. (A) Exocytosis via FCF. As with synaptotagmin I antibody-conjugated Qdots, the fluorescence within the ROI dropped suddenly to near-zero (33 s), indicating FCF. (B) 3D trace of a VGAT antibody-conjugated Qdot-labeled vesicle, corresponding to exocytosis via K&R. The fluorescence of the ROI showed a partial drop at 100 s (red arrow), indicating K&R, followed by near-complete loss of fluorescence at 120 s (black arrow), which indicated FCF.

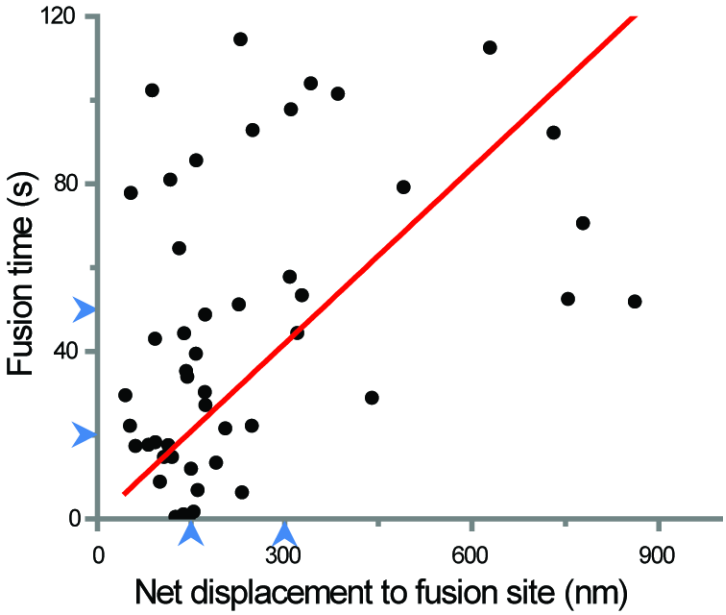

Fig. S4. Relationship between the net displacement to fusion site and the fusion time of vesicles loaded with 1200 APs. Vesicles located close to fusion sites were released earlier than those located further away ($p<0.005$ from the correlation analysis). The blue arrowheads indicate thresholds used for analysis of early and late releasing vesicles (Fig. 2A) and near- and far-positioned vesicles (Fig. 2B). The great majority of data were used in these analyses except 6 vesicles.

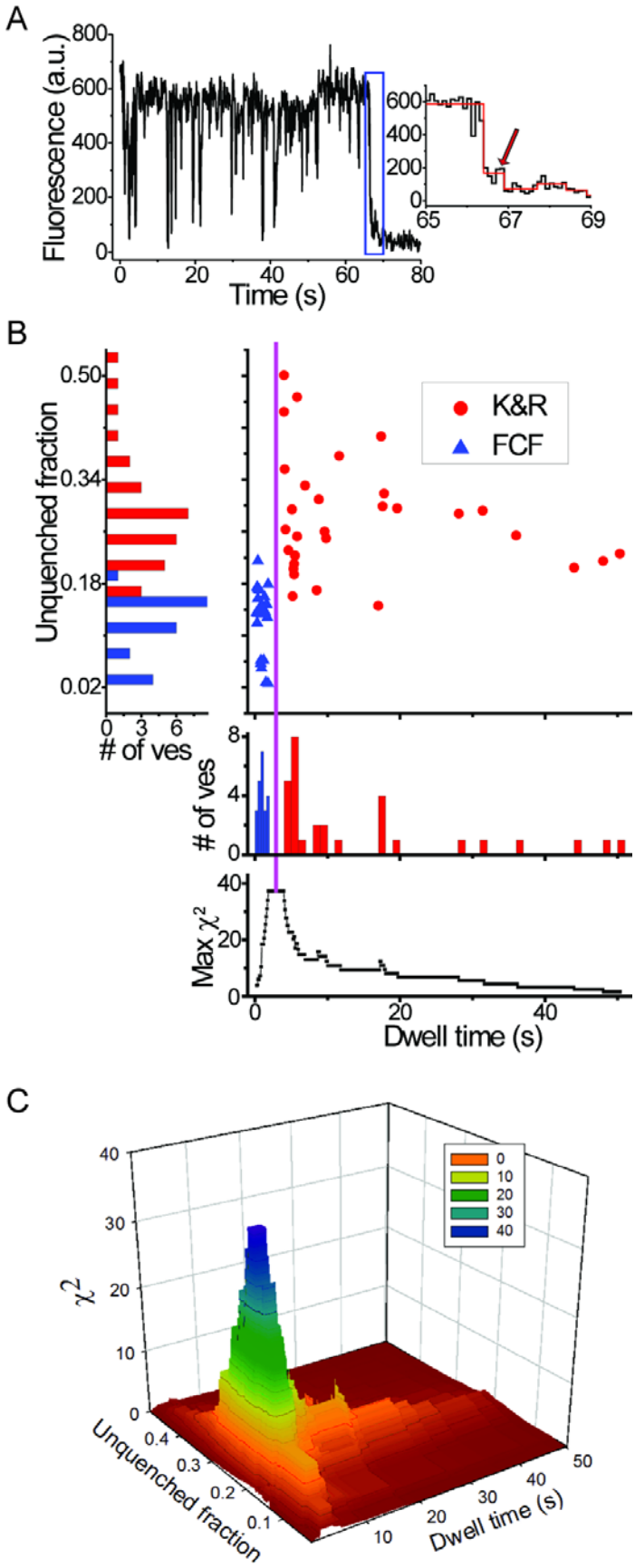
A
Fluorescence (a.u.)
800
600
400
200
0
0
20
40
60
80
Time (s)
600
400
200
0
65
67
69
B
Unquenched fraction
0.50
0.34
0.18
0.02
0
3
6
# of ves
K&R
FCF
8
4
0
# of ves
40
20
0
Max χ^2
0
20
40
Dwell time (s)
C
40
30
20
10
0
χ^2
0
10
20
30
40
0.4
0.3
0.2
0.1
Unquenched fraction
10
20
30
40
50
Dwell time (s)

Fig. S5. An analysis of the unquenched fraction and the dwell time. (A) A fluorescence trace of an ROI containing a Qdot-labeled vesicle, illustrating an apparent sojourn. The duration of the apparent sojourn (red arrow) was brief (0.4 s) compared with the long duration of the partial quenching sojourn in Fig. 3B. The inset shows an expanded view of the gradual decay of fluorescence as the Qdot moved away from the ROI after exocytosis. The red line represents the idealized fluorescence signal as calculated according to the *t*-test algorithm. (B) An analysis of the unquenched fraction and the dwell time at 1 μM TB. The data supported a clear distinction between two fusion modes: vesicles deemed to undergo FCF (blue triangles) have shorter dwell times and smaller unquenched fractions than those undergoing K&R (red circles). Lower panel, repeated χ^2 tests with variably positioned separators allowed us to obtain the greatest distinction between fusion modes (maximum χ^2 =37.3, $p < 10^{-8}$, for a dwell time separator positioned between 1.9 s and 4.0 s (magenta line)). (C) χ^2 values determined over the full range of variation in both dwell time and in unquenched fraction separators. The calculated χ^2 value peaked with a dwell time between 1.9 s and 4 s and an unquenched fraction between 0.179 and 0.194.

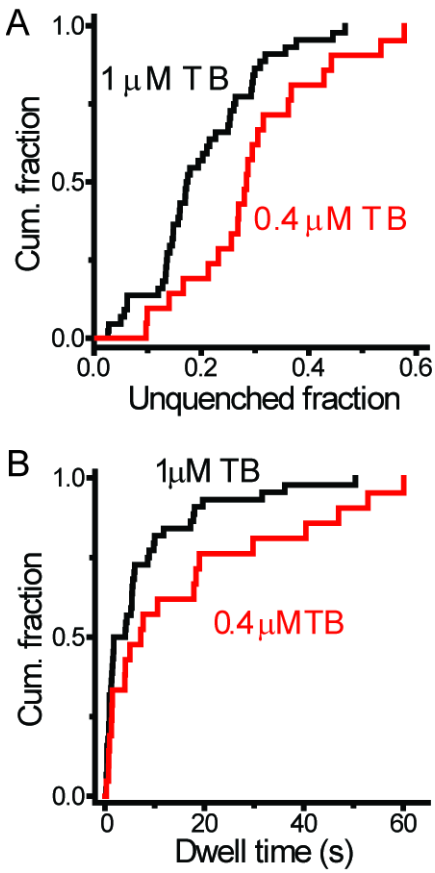

Fig. S6. The unquenched fraction and the dwell time at two different concentration of TB. (A) Unquenched fractions at 1 μM and 0.4 μM TB were significantly different ($p < 0.01$, K-S test), indicating that quenching fractions depend on the entry of TB. (B). Dwell times at 1 μM and 0.4 μM TB were not significantly different ($p > 0.2$, K-S test), suggesting that the kinetics of exocytosis and reuse were not different.

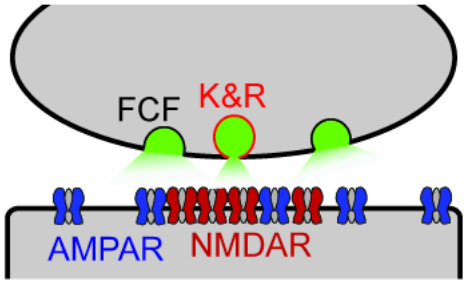

Fig. S7. A schematic representation of spatial alignment between fusion modes and glutamate receptors (NMDAR and AMPAR). K&R occurs opposite to NMDARs but away from the bulk of AMPARs, residing mostly in outer half of synaptic disk. FCF spread throughout, activates both NMDARs and AMPARs. Our spatial distribution of NMDAR and AMPAR was based on the reported distribution of NR1and GluR2/3(*16*, *17*).

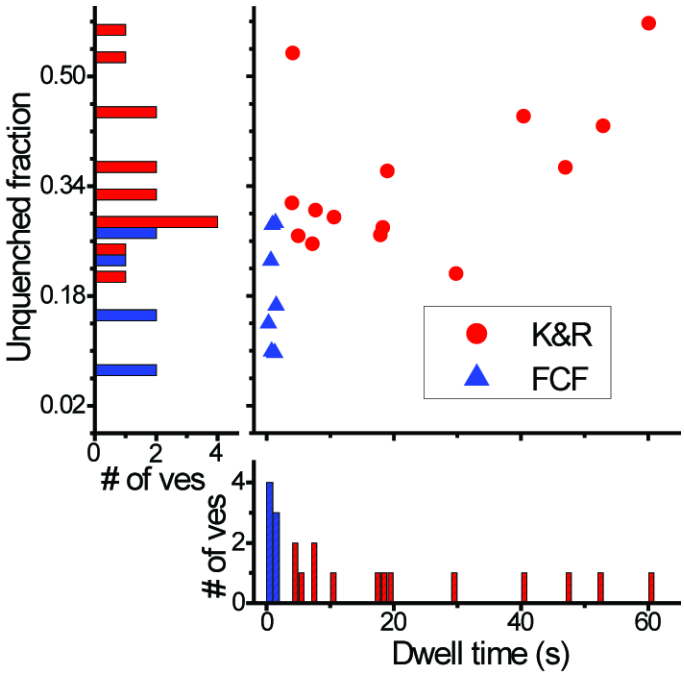

Fig. S8. The analysis of the dwell time and the unquenched fraction of exocytosed vesicles at 0.4 μM TB. As with 1 μM TB, the dwell time and the unquenched fraction were different between the two fusion modes: vesicles undergoing K&R have a longer dwell time and larger unquenched fraction than those undergoing FCF.

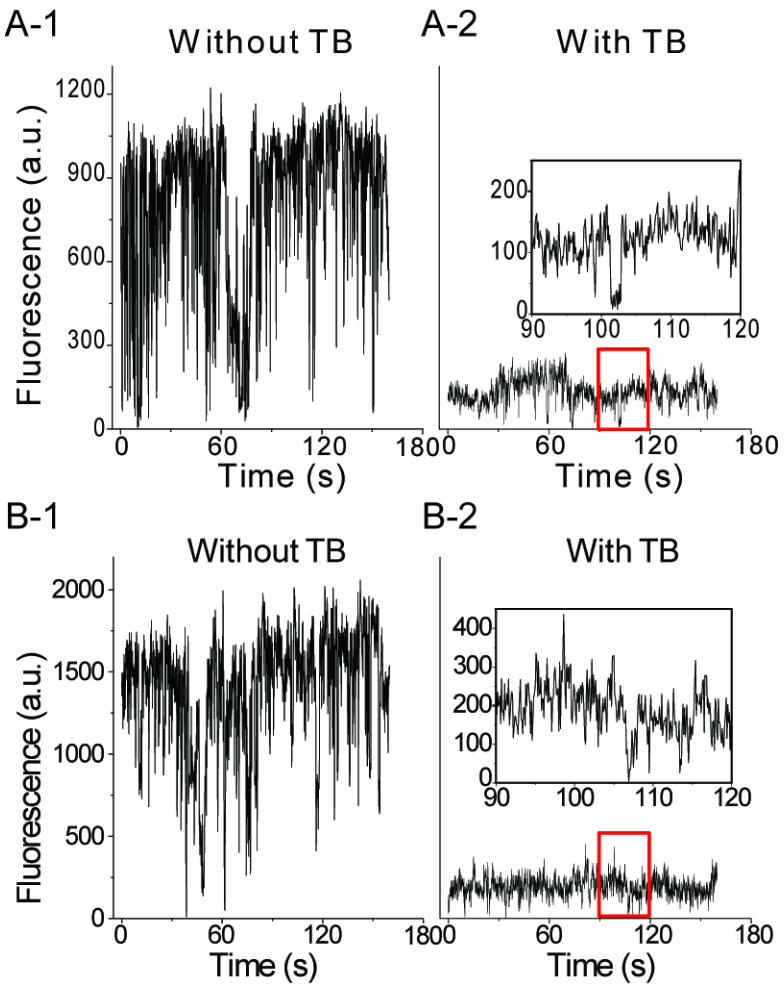

Fig. S9. *In vitro* assay of single Qdot fluorescence, determined with and without quencher. (A) Typical fluorescence traces of a single Qdot, obtained with and without quencher (TB). The fluorescence showed transient but nearly-complete loss of signal over multiple time intervals, implying that this fluorescence originated from a single Qdot. The addition of TB caused the fluorescence to drop (A-2). The inset is an expanded view. (B) Typical fluorescence traces of a single Qdot with or without quencher (TB), taken with a longpass emission filter (HQ500LP). The photoblinking proved that the fluorescence originated from a single Qdot. The addition of TB caused the fluorescence to drop (B-2). By virtue of its wider range of transmission wavelengths, the longpass emission filter yielded higher fluorescence intensity for Qdots than that obtained with a conventional emission filter. The inset is an expanded view.

References and Notes

1. S. O. Rizzoli, W. J. Betz, Synaptic Vesicle Pools. *Nat. Rev. Neurosci.* **6**, 57 (2005). doi:10.1038/nrn1583
2. A. M. Aravanis, J. L. Pyle, R. W. Tsien, Single synaptic vesicles fusing transiently and successively without loss of identity. *Nature* **423**, 643 (2003). doi:10.1038/nature01686
3. S. P. Gandhi, C. F. Stevens, Three modes of synaptic vesicular recycling revealed by single-vesicle imaging. *Nature* **423**, 607 (2003). doi:10.10.1038/nature01677
4. D. A. Richards, Vesicular release mode shapes the postsynaptic response at hippocampal synapses. *J. Physiol.* **587**, 5073 (2009). doi:10.1113/jphysiol.2009.175315
5. Q. Zhang, Y. Li, R. W. Tsien, The Dynamic Control of Kiss-And-Run and Vesicular Reuse Probed with Single Nanoparticles. *Science* **323**, 1448 (2009). doi:10.1126/science.1167373
6. N. C. Harata, S. Choi, J. L. Pyle, A. M. Aravanis, R. W. Tsien, Frequency-Dependent Kinetics and Prevalence of Kiss-and-Run and Reuse at Hippocampal Synapses Studied with Novel Quenching Methods. *Neuron* **49**, 243 (2006). doi:10.1016/j.neuron.2005.12.018
7. P. V. Berghe, J. Klingauf, Synaptic vesicles in rat hippocampal boutons recycle to different pools in a use-dependent fashion. *J. Physiol.* **572**, 707 (2006). doi:10.1113/jphysiol.2005.100842
8. B. Huang, W. Wang, M. Bates, X. Zhuang, Three-Dimensional Super-Resolution Imaging by Stochastic Optical Reconstruction Microscopy. *Science* **319**, 810 (2008). doi:10.1126/science.1153529
9. T. M. Watanabe, T. Sato, K. Gonda, H. Higuchi, Three-dimensional nanometry of vesicle transport in living cells using dual-focus imaging optics. *Biochem. Biophys. Res. Commun.* **359**, 1 (2007). doi:10.1016/j.bbrc.2007.04.168
10. G. Shtengel *et al.*, Interferometric fluorescent super-resolution microscopy resolves 3D cellular ultrastructure. *Proc. Natl. Acad. Sci. U.S.A.* **106** 3125 (2009). doi:10.1073/pnas.0813131106
11. M. Howarth *et al.*, Monovalent, reduced-size quantum dots for imaging receptors on living cells. *Nat. Methods* **5**, 397 (2008). doi:10.1038/NMETH.1206
12. K. J. Darcy, K. Staras, L. M. Collinson, Y. Goda, Constitutive sharing of recycling synaptic vesicles between presynaptic boutons. *Nat. Neurosci.* **9**, 315 (2006). doi:10.1038/nn1640
13. A. Denker, S. O. Rizzoli, Synaptic vesicle pools: an update. *Front. Syn. Neurosci.* **2**, 1 (2010). doi:10.3389/fnsyn.2010.00135synapses
14. S. O. Rizzoli, W. J. Betz, The Structural Organization of the Readily Releasable Pool of Synaptic Vesicles. *Science* **303**, 2037 (2004). doi:10.1126/science.1094682
15. T. Schikorski, C. F. Stevens, Morphological correlates of functionally defined synaptic vesicle populations. *Nat. Neurosci.* **4**, 391 (2001). doi:10.1038/86042
16. V. N. Kharazia, R. J. Weinberg, Tangential synaptic distribution of NMDA and AMPA receptors in rat neocortex. *Neurosci. Lett.* **238**, 41 (1997).
17. P. Somogyi, G. Tamás, R. Lujan, E. H. Buhl, Salient features of synaptic organisation in the cerebral cortex. *Brain Res. Rev.* **26**, 113 (1998).
18. A. Dani, B. Huang, J. Bergan, C. Dulac, X. Zhuang, Superresolution Imaging of Chemical Synapses in the Brain *Neuron* **68**, 843 (2010). doi:10.1016/j.neuron.2010.11.021
19. V. V. Uteshev, P. S. Pennefather, Analytical Description of the Activation of Multi-State Receptors by Continuous Neurotransmitter Signals at Brain Synapses. *Biophys. J.* **72** 1127 (1997). doi:10.1016/S0006-3495(97)78761-7

20. K. M. Franks, C. F. Stevens, T. J. Sejnowski, Indepent sources of quantal variablity at single glutamatergic synapse. *J. Neurosci.* **23**, 3186 (2003).
21. J. S. Diamond, C. E. Jahr, Transporters Buffer Synaptically Released Glutamate on a Submillisecond Time Scale. *J. Neurosci.* **17**, 4672 (1997).
22. S. Choi, J. Klingauf, R. W. Tsien, Fusion pore modulation as a presynaptic mechanism contributing to expression of long-term potentiation. *Philos. Trans. R. Soc. London Ser. B* **358**, 695 (2003). doi:10.1098/rstb.2002.1249
23. G. Liu, R. W. Tsien, Synaptic transmission at single visualized hippocampal boutons. *Neuropharmacology* **34**, 1407 (1995). doi:10.1016/0028-3908(95)00143-T
24. M. Jiang, G. Chen, High Ca2+-phosphate transfection efficiency in low-density neuronal cultures. *Nat. Protoc.* **1**, 695 (2006). doi:10.1038/nprot.2006.86
25. F. Pinaud, S. Clarke, A. Sittner, M. Dahan, Probing cellular events, one quantum dot at a time. *Nat. Methods* **7**, 275 (2010). doi:10.1038/nmeth.1444
26. S. Roseth, E. M. Fykse, F. Fonnum, Uptake of L-Glutamate into Synaptic Vesicles: Competitive Inhibition by Dyes with Biphenyl and Amino- and Sulphonic Acid-substituted Naphthyl Groups. *Biochem Pharmacol* **56**, 1243 (1998).
27. C. Kural *et al.*, Tracking melanosomes inside a cell to study molecular motors and their interaction. *Proc. Natl. Acad. Sci. U.S.A.* **104**, 5378 (2007). doi:10.1073/pnas.0700145104
28. N. J. Carter, R. A. Cross, Mechanics of the kinesin step. *Nature* **435**, 308 (2005). doi:10.1038/nature03528
29. G. E. Snyder, T. Sakamoto, I. John A. Hammer, J. R. Sellers, P. R. Selvin, Nanometer Localization of Single Green Fluorescent Proteins: Evidence that Myosin V Walks Hand-Over-Hand via Telemark Configuration. *Biophys. J.* **87**, 1776 (2004). doi:10.1529/biophysj.103.036897
30. L. He, X.-S. Wu, R. Mohan, L.-G. Wu, Two modes of fusion pore opening revealed by cell-attached recordings at a synapse. *Nature* **444**, 102 (2006). doi:10.1038/nature05250
31. S. F. Lee, M. A. Osborne, Brightening, Blinking, Bluing and Bleaching in the Life of a Quantum Dot: Friend or Foe?, *ChemPhysChem* **10**, 2174 (2009). doi:10.1002/cphc.200900200
32. S. F. Lee, M. A. Osborne, Photodynamics of a Single Quantum Dot: Fluorescence Activation, Enhancement, Intermittency, and Decay, *J. Am. Chem. Soc.* **129**, 8936 (2007). doi:10.1021/ja071876+
33. J. L. Pyle, E. T. Kavalali, E. S. Piedras-Renteria, R. W. Tsien, Rapid Reuse of Readily Releasable Pool Vesicles at Hippocampal Synapses. *Neuron* **28**, 221 (2000). doi:10.1016/S0896-6273(00)00098-2
34. Q. Zhang, Y.-Q. Cao, R. W. Tsien, Quantum dots provide an optical signal specific to full collapse fusion of synaptic vesicles, *Proc. Natl. Acad. Sci. U.S.A.* **104**, 17843 (2007). doi:10.1073/pnas.0706906104
35. N. Harata, T. A. Ryan, S. J. Smith, J. Buchanan, R. W. Tsien, Visualizing recycling synaptic vesicles in hippocampal neurons by FM 1-43 photoconversion. *Proc. Natl. Acad. Sci. U.S.A.* **98**, 12748 (2001). doi:10.1073ypnas.171442798